Environ Geochem Health (2025) 47:396
https://doi.org/10.1007/s10653-025-02711-6

ORIGINAL PAPER

Antimony sources and mobilization in environmental matrices surrounding the world's largest Sb mine: evidence from mineralogy and Sb isotope signatures

Taoran Shi · WenJing Guo · Guangyi Sun · Jining Li · Jin Ma · Min Sun · Yutong Ji · Chunfa Wu

Received: 17 March 2025 / Accepted: 31 July 2025 / Published online: 18 August 2025
© The Author(s), under exclusive licence to Springer Nature B.V. 2025

Abstract China produces 48.2% of global antimony (Sb) annually, of which approximately 80% was produced in Southwest China in 2023. The distribution of high-Sb geological background areas in China overlaps with that of karst landforms. The external causes of the exploitation and utilization of Sb resources and the internal causes of the special high geochemical background have led to Sb pollution in the natural ecosystems in this area. This study selected the Xikuangshan (XKS) Sb mine in Hunan Province, a typical Sb deposit in the karst areas of China, as an example to quantitatively identify pollution sources and influencing factors of Sb in the environment around the Sb mining area. Based on the TESCAN integrated mineral analyzer analysis, the major mineralogical components of the representational soil sample were quartz (59.80%), kaolinite (9.93%), calcite (6.08%), albite (3.41%), chlorite-clinochlore (2.89%), clay (1.99%), dolomite (1.81%), and hematite (Fe_2O_3)/magnetite (Fe_3O_4) (1.67%). Antimony was found to be mainly rich in Fe_2O_3/Fe_3O_4, nepheline ($NaAlSiO_4$), and minerals consisting of O-Al-Si or O-S-Fe in the soil. Based on microscopic X-ray fluorescence analysis, Sb showed similar in situ distribution and enrichment characteristics to those of Al, Fe, S, and Si. The characteristics of the Sb isotope of the environmental samples from the XKS Sb mine were measured for the first time. A large variation in $\delta^{123}Sb$ values and chemical species fractions of Sb in soil samples suggests that Sb in soils from different geographical location may have different origins or migration behaviors. The Sb isotope composition of soil can be divided into four endmembers: atmospheric deposition, tailing leaching, river water surface

Supplementary Information The online version contains supplementary material available at https://doi.org/10.1007/s10653-025-02711-6.

T. Shi (✉) · M. Sun · Y. Ji · C. Wu (✉)
School of Ecology and Applied Meteorology, Nanjing University of Information Science & Technology, Nanjing 210044, China
e-mail: shitaoran@126.com

C. Wu
e-mail: wchf1680@sina.com

W. Guo
Institute of Agricultural Resources and Environment, Jiangsu Academy of Agricultural Sciences, Nanjing 210014, China

G. Sun
State Key Laboratory of Environmental Geochemistry, Institute of Geochemistry, Chinese Academy of Sciences, Guiyang 550081, China

J. Li
Institute of Eco-Environmental and Soil Sciences, Guangdong Academy of Sciences, Guangzhou 510650, China

J. Ma
State Key Laboratory of Environmental Criteria and Risk Assessment, Chinese Research Academy of Environmental Sciences, Beijing 100012, China

runoff, and rock oxidative weathering. The differences in hydrochemical types and Sb isotopic signatures among river waters indicate multiple sources and factors influencing Sb migration in different locations. The Sb in river water may have been partly influenced by rock leaching. Sweet potato exhibited a similar Sb isotopic signature ($\delta^{123}Sb = 0.24‰$) with surrounding soil ($\delta^{123}Sb = 0.22‰$), which demonstrated that the sweet potato absorbed Sb through contaminated soil to the root. Soil erosion and tailings are the major sources of Sb in street dust. A conceptual model was established to elucidate the pollution sources and the main geochemical processes affecting the mobilization of Sb in environmental matrices in the XKS mining area. This study provides a scientific basis for environmental quality assessment of Sb mining areas and establishment of an effective early warning system for Sb pollution in soil.

Keywords Antimony isotope · Soil · Xikuangshan Sb mine · Geochemical process · Source apportionment

Introduction

Antimony (Sb), a widely distributed metalloid element with chronic toxicity to living organisms and long-distance transportation, has garnered the attention of researchers due to its pollution and migration behavior (Bolan et al., 2022; Zhou et al., 2023). Antimony and its compounds are listed as priority pollutants by the US EPA and the European Union. It has been listed as one of the key pollutants in the second category of comprehensive control of potentially toxic elements (PTEs) pollution in China. Antimony reserves and production of China rank first worldwide. China accounts for 31.30% of global Sb reserves, and 48.19% of global Sb production in 2023 (USGS, 2023). China plays the most important role in global Sb emissions (Chu et al., 2019). Antimony resources are mainly distributed in the Southwest of China, accounting for over 80% of the country's total Sb reserves. Southwest China is an important area for the low-temperature metallogenesis of nonferrous metals. The soil background value in southwest China is significantly higher than the national average level, which is mainly due to the high background value formed by endogenous parent material and natural soil formation process in karst limestone area (Fig. S1). The geogenic sources of the special high geochemical background coupled with the anthropogenic sources of intensification of mining activity have led to notable environmental problems related to Sb pollution in this area (He et al., 2012; Li et al., 2018; Liu et al., 2024b; Qin et al., 2022; Ren et al., 2019; Wu et al., 2019). When comparing the health risks of soil PTEs in different types of mining areas in China, the Sb mine was identified as the primary control mine (Li et al., 2014).

Source identification of PTEs is the precondition of preventing and controlling pollution. On November 7, 2024, the Ministry of Ecology and Environment of the People's Republic of China issued the Action Plan for Soil Pollution Sources Prevention and Control. Potentially toxic elements pollution in cultivated soil in China mainly comes from industries such as non-ferrous metal smelting and mining. The lack of scientific understanding of the contribution and mechanism of natural and anthropogenic sources to the accumulation of Sb in soil, to some extent, limited the scientific understanding of existing strategies for the control of Sb pollution in soil. Sb can be adsorbed by clay minerals, organic matter (OM), and Al, Fe, and Mn oxides in the soil, which affects the mobility of soil Sb (Zhang et al., 2022a). SEM–EDS has shown that the distribution of Sb and Ca in soil was similar (Zhou et al., 2024). Antimony content in soil is positively related to the contents of silicate minerals and quartz (García-Lorenzo et al., 2015). Therefore, the analysis of soil mineral composition, the distribution of Sb in mineral phases, and the controlling effect of mineral composition on the distribution characteristics of Sb are needed to identify the source of Sb in soil from a microscopic point of view. Antimony has two stable isotopes, ^{121}Sb (57.213%) and ^{123}Sb (42.787%), which have large masses and a relatively small fractionation range (Aston, 1923). Antimony isotopes are non-traditional stable isotopes and their fractionation scale is smaller than that of other isotopes. Traditional isotopes, such as S, H, O, Hg, Sr, Pb, and Mo have been widely applied to identify the sources and predominant geochemical processes of Sb in the environment (Fu et al., 2020; Hao et al., 2022; Song et al., 2022; Wen et al., 2023a; Yang et al., 2006). As the MC-ICP-MS develops, precise measurements of Sb isotopic compositions have become possible (Rouxel et al., 2003; Sun et al.,

Buy me a coffee https://ko-fi.com/jurnalin https://dbook.eu.org

2021). The mechanisms of Sb isotope fractionation currently include biological (Ferrari et al., 2023; Jia et al., 2024), reduction (Wang et al., 2021a, 2021b), adsorption (Ferrari et al., 2024; Zhou et al., 2023), evaporation (Chen et al., 2024), precipitation (Yu et al., 2023), weathering (Kaufmann et al., 2024) and mixing processes. Although there have been many studies on the uptake and transport of Sb by plants, the fractionation of Sb isotopes in this biological process has not been reported. Similar to most elements, plants preferentially absorb and transport light Sb isotopes in the soil–plant system, resulting in heavy Sb isotopic composition in the rhizosphere (Liao et al., 2023). Isotope fractionation of natural source Sb may be controlled by plant uptake (Liao et al., 2023).

The XKS Sb mine, the largest Sb mine in the world, was selected for a detailed Sb isotope study because of its historical Sb contamination in karst areas (Wen et al., 2023a, 2023b). Recently, numerous researches have been carried out systematically in the field of Sb pollution in single environmental media, such as soil (Liao et al., 2023; Wang et al., 2022), aquatic systems (Liu et al., 2023; Sheng et al., 2023; Wen et al., 2023b), sediment (Zhang et al., 2022b), tailings (Li et al., 2022), stibnite (Yu et al., 2023; Zhai et al., 2021) and crops (Gaiss et al., 2019) in XKS. Rock-soil (Zhou et al., 2023), rock-water (Hao et al., 2022), water–sediment (Zhou et al., 2024), and soil–plant (Pervaiz et al., 2023) are the most active interfaces of the Sb bio-geochemical cycling in supergene environments. However, geochemical cycles of Sb in environmental systems remain poorly understood. The purposes of this study were to (1) explore the chemical species, existing state in minerals, in situ distribution, and enrichment characteristics of Sb in environmental matrices, (2) analyze the Sb isotopic signatures of different environmental compartments, and (3) elucidate the pollution sources of Sb and geochemical processes affecting Sb migration. This study provides a basis for further research on long-distance migration and transformation of Sb in environmental systems.

Materials and methods

Study area and sample collection

This study was carried out in the XKS Sb mine (N27.7°, E111.4°) located in Lengshuijiang City, Hunan Province, China and known as "World Capital of Sb." The XKS deposit covers 16 km^2 and includes the North and South mines. Currently, the North mine is a smelting area, and the South mine is a mining area. The history of Sb mining in XKS goes back to the nineteenth century, with the first Sb smelter being built in 1897, and mining activities continue to today. The local Qingfeng and Xuanshan Rivers and the Batangshan, Feishuiyan, and Tanjia Streams all originate from the XKS mine and eventually flow into the Zijiang River in Hunan. Two major rivers exist, the Qingfeng and Lianxi Rivers, which are tributaries of Zijiang River (Fig. S2). Both flow through the mining region and receive large amounts of mining and smelting wastewater. The most abundant mineral in this mine is stibnite (Sb_2S_3).

Multiple environmental matrices samples were collected in October 2022, including soil (n = 21), unmineralized rock (n = 2), surface river water (n = 6), sediment (n = 5), dust (n = 2), tailing (n = 1), maize grain (n = 3), and sweet potato (n = 2). Surface sediment samples corresponding to the river water samples (no sediment samples in some locations) were collected. This study particularly focused on biogeochemical cycle of Sb in soil. The spatial heterogeneity of rocks are not conspicuous, two samples were selected to represent the mine area lithology. Tailings were collected in mining area from a centralized piled tailing heap. Sweet potatoes and corns were collected incidentally. The spatial heterogeneity of dusts reflecting atmospheric deposition in mining area are also not conspicuous. The sample sites were located near two major ore deposits along the two rivers. The locations of the sampling sites are shown in Fig. 1 and the site descriptions are shown in Table S1. Surface soil samples (0–20 cm) were collected with a soil auger. Dust samples were collected from tree leaves on mining roads using plastic brush and spades. The tailings were collected from the top and bottom of a tailing heap using 50 mL sterile centrifuge tubes. Rock samples with fresh and unaltered faces were collected from outcrops using a geological hammer. Maize grains were collected from granaries of local

Buy me a coffee https://ko-fi.com/jurnalin https://dbook.eu.org

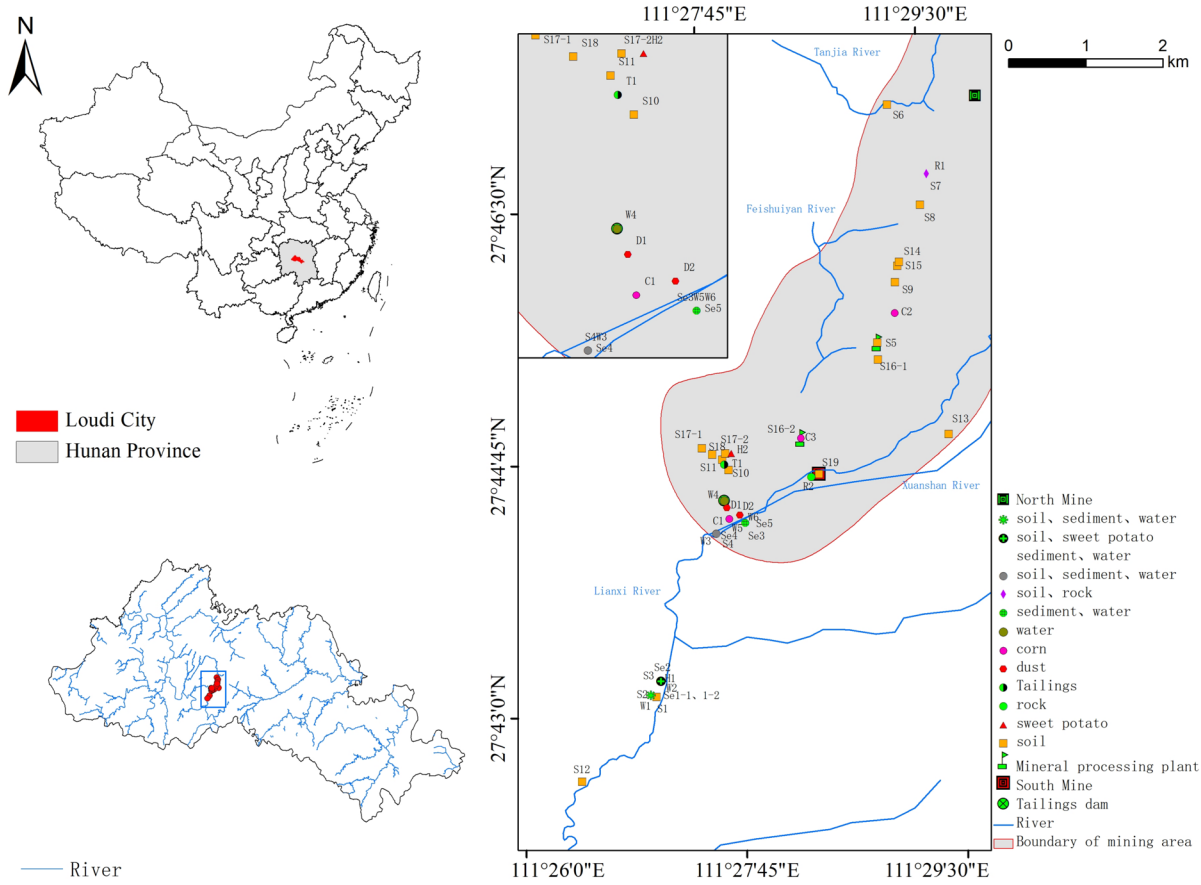

Fig. 1 Study area and locations of sampling sites

residents. Sweet potatoes were collected in the mature period from farmland surrounding the mine area.

Sample processing and analysis

Physicochemical properties of solid samples

Soil, sediment, dust, and tailing samples were air-dried and litter and root mats were removed from the solid samples, crushed, passed through a nylon sieve of 100 meshes, and stored at − 4 ℃. The rock samples were crushed to < 200 mesh using a ball grinder. (i) The pH, dissolved oxygen (DO), electrical conductivity (EC), and oxidation–reduction potential (Eh) were determined in a 1:2.5 soil/water suspension using water quality field meters (YSI Pro Plus, USA). (ii) Total Sb concentrations determination: following the microwave digestion (MARS, CEM, USA) of the solid samples with HNO_3 + HF (3:1), the total Sb concentrations were determined using hydride generation atomic fluorescence spectrometry (HG-AFS) (AFS 9700, Titan Instrument Co., Ltd., China). (iii) Soil OM content was determined according to the national standard method (GB9834-88). (iv) Soil mineral composition: The mineral composition of soil sample was investigated by X-ray diffraction (XRD) using a Bruker AXS D8 Discover microdiffractometer. Soil samples were prepared as standard petrology slices for mineral identification using a TESCAN integrated mineral analyzer (TIMA) (TESCAN ORSAY HOLDING, a.s) and M4 TORNADO microscopic X-ray fluorescence analyzer (μ-XRF) (Bruker, Germany). (v) Sb fraction in the soils: Sb fractions were determined using the modified Community Bureau of Reference (BCR) sequential extraction procedure. It classifies soil metals into three major fractions: exchangeable (F1), reducible (F2), and oxidizable (F3), with the residue (F4) modified by aqua

Buy me a coffee https://ko-fi.com/jurnalin https://dbook.eu.org

regia digestion (Rauret et al., 1999). (vi) Sb chemical speciation: Sb(III), Sb(V), and trimethylantimony (TMSb) in the samples were analyzed using HG-AFS (SA-10 Titan Instrument Co. Ltd., Beijing, China). The detection limit of Sb(III), Sb(V), and TMSb was 0.2 mg/kg.

Physicochemical properties of water samples

River water samples were filtered with 0.45 μm Teflon membranes and kept in 500 mL HDPE bottles, which were rinsed twice with deionized water and three times with filtered water samples before sampling. Filtered samples used to measure major ions, total Sb concentration and Sb isotopes were acidified to pH < 2 with ultrapure HNO_3. (i) The pH, DO, EC, and Eh were determined using water quality field meters (YSI Pro Plus, USA). (ii) Major cation and anion concentrations determination: K^+, Na^+, Ca^{2+}, Mg^{2+}, F^-, Cl^-, NO_3^-, SO_4^{2-}, and PO_4^{3-} concentrations in the river water were determined using ion chromatography (Dinex-100). The HCO_3^- concentrations were determined using the neutralization titrimetric method. Based on the equilibrium relationship between CO_3^{2-} and HCO_3^- dissolved in water, the CO_3^{2-} content was negligible in this study. (iii) Total Sb concentrations determination: The digestion and determination methods are as described in the previous section (iv) Sb chemical speciation: The method is as described in the previous section. The detection limits of Sb(III), Sb(V), and TMSb was 0.1 μg/L, 0.5 μg/L, and 0.5 μg/L respectively.

Physicochemical properties of biological samples

Sweet potato tissues were vacuum freeze-dried, ground, passed through a 100 mesh screen, and kept at − 4 ℃. The maize grain samples were ground, sifted through a nylon sieve of 100 meshes, and kept in polyethylene flasks until digestion. Total Sb concentrations determination: The digestion and determination methods are as described in the previous section.

Sb isotopes

The Sb isotopic compositions of the samples were analyzed in low-resolution mode using Nu plasma II MC-ICP-MS with membrane desolvation (Aridus II) and a HG system in the Institute of Geochemistry, Chinese Academy of Science. The detailed purification process and determination methods are presented (Sun et al., 2021). Sb-containing reference standard (NIST SRM 3102a) made in the National Institute of Standards and Technology was selected for the analysis of Sb isotopes.

Sb isotope data is represented by a delta (δ) value, expressed as a difference per million (‰) relative to the standard:

$$\delta 123\mathrm{Sb} = \left[\frac{\left(123_{Sb}/121_{Sb}\right)_{\text{sample}}}{\left(123_{Sb}/121_{Sb}\right)_{\text{standard}}} - 1 \right] \times 1000$$

Quality control

Digestion procedures were conducted in triplicate and the standard reference material (river sediment, GBW07360) was digested simultaneously. The relative error of the replicates was less than 10% and the recovery of the reference materials ranged from 90 to 110%. For modified BCR, the total recovery ranged from 88 to 120%. For isotopic analysis of Sb, the instrument error was controlled by the sample standard surround method and element doping, with an accuracy of 0.4 ε (2SD).

Results and discussion

Sb contamination in environment matrices

Soil

The total Sb concentration in the soil ranged from 1.29 to 1,671 mg/kg, with an average of 365.3 mg/kg (n = 21), exceeding the background value (1.23 mg/kg) in Chinese soil (CNEMC, 1990) at all sampling sites. The average Sb concentrations in the soils from the XKS mine were compared with those of other typical Sb mines or deposits in China and abroad, and the Sb concentration was between the 50th and 75th percentiles (Fig. S3). The Sb concentrations in 85.7% of the soil samples from the XKS mine were higher than the toxicity guidelines recommended by World Health Organization for soil Sb (WHO, 36 mg/kg). The Sb concentrations in 95.2% and 81.0% of the soil samples exceeded the risk screening values of

Buy me a coffee https://ko-fi.com/jurnalin https://dbook.eu.org

20 mg/kg and 40 mg/kg, respectively, whereas 61.9% and 33.3% of the soil samples had Sb concentrations exceeding the intervention values of 180 mg/kg and 360 mg/kg, respectively, for soil contamination of the two types of development land (GB36600-2018). The pH value of the soil ranged from 4.92 to 7.23, with an average value of 6.57. More than 90% of the soil samples were acidic, which may have worsened the degree of PTEs contamination.

River water

The concentrations of Sb in unpolluted water are generally less than 1 µg/L (Nelson et al., 2011), mainly due to the low solubility of Sb minerals. In this study, river water had a wide range of total Sb concentration ranging from 1.2 to 1,020 µg/L, with the mean value of 410.1 µg/L (n = 6). It exceeded the Chinese drinking water standard (5 µg/L) and US EPA standard limit for drinking water (6 µg/L) 82 and 68 times, respectively. Samples W3 (680 µg/L), W4 (750 µg/L), and W5 (1,020 µg/L) showed higher Sb concentrations, which may be due to point source pollution, such as the tailings dam located near the W4 site. The concentration of Sb in river water from XKS was reported to be 16–2,137 µg/L (Guo et al., 2018). The total Sb concentration was 2–6,384 µg/L, 224–2,099 µg/L, and 6–240 µg/L in Qingfeng River, Lianxi River, and Zijiang River, respectively. (Wang et al., 2011). The total Sb concentrations ranged from 1.45 µg/L to 15.66 µg/L in the Zijiang surface waters (Liu et al., 2023). Spatially, the Sb concentration showed a downward trend from the tributaries to the main stream of Zijiang River (Liu et al., 2023).

A considerable variation was observed in the pH of the river water from the XKS mine area, with pH values ranging from 3.23 to 8.34, with an average value of 6.4 (Table 1). Similarly, Sheng et al. (2022) reported that the average pH value of sampling points affected by mining was 7.67 (6.57–8.08), and the water environment was generally neutral or weakly alkaline (Sheng et al., 2022). The pH values of river water from XKS reported by Wen et al., (2023a, 2023b) indicated that the river water was alkaline (8.06 to 8.80). The pH values of river water from XKS in this study were lower than that in existing studies. The most probable reason is differences in sampling locations with varying pollution levels. The oxidation of FeS_2 and FeAsS and the dissolution of certain secondary minerals made the river water acidic in the mine area. The interaction of water with carbonate rocks can neutralize any potential acidity resulting from the sulfide minerals oxidation associated with the Sb ore (Nyirenda et al., 2015).

Table 1 Physicochemical properties and common ions concentration in river water

Samples	Sb µg/L	pH /	Eh mv	DO mg/L	EC µS/cm	HCO_3^- mg/L	Na^+ mg/L	K^+ mg/L
W1	1.40	3.41	404.1	7.35	1786	26.18	20.39	11.42
W2	1.20	3.23	439.2	7.35	1856	20.84	22.55	12.22
W3	680	8.08	214.6	7.18	997	40.07	40.45	10.18
W4	750	7.78	185.2	7.02	1380	37.40	80.91	20.36
W5	1020	8.34	170.9	7.22	861	14.43	47.64	9.50
W6	8.10	7.56	181.6	7.09	233	24.58	8.26	6.92
Samples	Ca^{2+} mg/L	Mg^{2+} mg/L	F^- mg/L	Cl^- mg/L	SO_4^{2-} mg/L	NO_3^- mg/L	PO_4^{3-} mg/L	NO_2^- mg/L
W1	322.27	53.26	0.46	7.39	1188.33	8.84	N.D	N.D
W2	350.59	56.59	0.49	9.57	1298.35	9.74	N.D	N.D
W3	161.47	11.23	1.73	27.46	431.79	6.54	N.D	N.D
W4	322.94	22.45	1.92	15.60	677.60	13.08	N.D	N.D
W5	137.47	5.77	1.36	34.03	370.51	5.41	N.D	N.D
W6	33.63	4.76	0.19	9.55	21.84	7.37	N.D	N.D

N.D. not detected

Buy me a coffee https://ko-fi.com/jurnalin https://dbook.eu.org

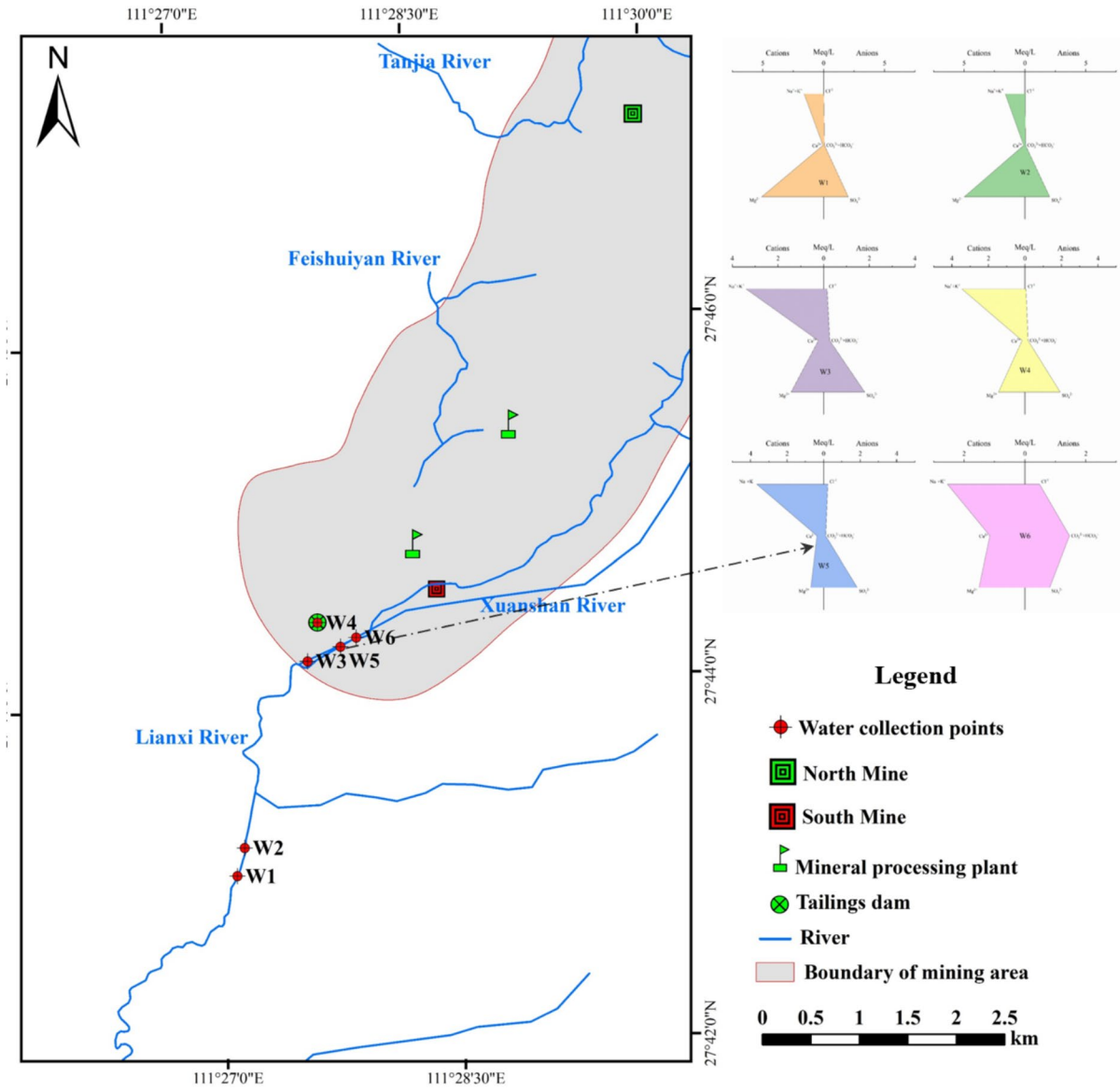

Fig. 2 GIS-Stiff diagram of river water showing change of dominant ions from W1 to W6

As indicated by the GIS-Stiff diagram (Fig. 2) for the river water, W1 to W5 samples were classified as the SO_4-Ca type. The W3, W4, and W5 samples had higher Sb and lower SO_4^{2-} concentrations compared with W1 and W2 samples. The major source contributing to SO_4^{2-} is the direct oxidative dissolution of Sb_2S_3 ores, as shown in the following equation (Cidu et al., 2018):

$$Sb_2S_3(s) + 7O_2(aq) + 10H_2O \rightarrow 2Sb(OH)_6^-(aq) + 3SO_4^{2-}(aq) + 8H^+(aq)$$

Sample W6 was classified as the HCO_3-SO_4-Ca type. A previous study indicated that river water samples could be classified as Ca-SO_4 type (Wen et al., 2016). Hydrogeochemistry and Sb pollution sources

Buy me a coffee https://ko-fi.com/jurnalin https://dbook.eu.org

in river water are more complicated in mining areas. The non-carbonate hardness (secondary salinity) of W1 and W2 was greater than 50%, and the non-carbonate alkali metal (primary salinity) of W3 to W6 was greater than 50%. The total Sb concentrations were positively correlated with F^- and Cl^- ($p < 0.05$), however, not significant with SO_4^{2-} in the river water (Table S2). As aforementioned, the inconsistency between SO_4^{2-} and Sb concentrations indicates that the sources of SO_4^{2-} in the water were mining and smelting activities or the lithology of the mine area (Wang et al., 2011).

Sediment

The total Sb concentration in the sediment ranged from 209 to 3,032 mg/kg with an average of 1,216 mg/kg (n = 5). It has been reported that the total Sb concentration was 57.11–7,315.7 mg/kg in the sediment from XKS (Wang et al., 2011). The total Sb concentrations were 3.16–133.63 mg/kg in the Zijiang sediments (Liu et al., 2023). The sediment toxicity guidelines for Sb set by Australia are 25 mg/kg (ANZECC, 2000), and the maximum permissible concentration is 19 mg/kg in the Netherlands (Crommentuijn et al., 1997). Mining, mineral processing, and smelting activities have caused serious damage to the ecological environment in XKS. The total Sb concentration in the sediment was distributed nonuniformly. The highest Sb concentration in the Se3 sample corresponding to river water sample W5 had the highest Sb concentration. The Sb concentrations in midstream were proved to be higher than that in upstream and downstream (Liu et al., 2023).

Dust, rock, and tailings

The total Sb concentrations in street dust were 957 mg/kg and 1,377 mg/kg, with an average value of 1,167 mg/kg (n = 2). Few related studies have been conducted on Sb levels in dust from Sb mine areas. Sb concentration was between 1.05 and 479.38 mg/kg in road dust from Daye Copper Smelter in Hubei Province, China (Wang et al., 2021a, 2021b). Large-scale industrial activities emit large amounts of Sb as particulate pollutants.

The total Sb concentration in rock was 1.18 and 1.68 mg/kg, with an average value of 1.43 mg/kg (n = 2). The concentration of Sb in rocks is generally between 0.15 and 2 mg/kg (Pierart et al., 2015). Geogenesis is the primary source of environmental Sb contamination (Herath et al., 2017). The concentration of Sb in limited rock samples from XKS did not increase. To date, there is limited information on the migration mechanisms of Sb from host mineral phases and their transformation in different environmental compartments.

The total Sb concentration in the tailing from XKS was 1,537 mg/kg (n = 1). The total Sb concentration in tailings from XKS ranged from 684 to 17,196 mg/kg (Fu et al., 2016). These results suggest that tailing piles are a potential source of Sb in water and soils because the tailings were left untreated and stacked in open air with no boundary with soil. Radková et al. (2020) found that the interactions between water and tailings are vital processes that affect the release and transfer of Sb from point pollution source into rivers.

Crop

The total Sb concentrations in the edible parts of the crop samples from XKS were measured. The total Sb concentrations in corn grains were 0.74, 1.90, and 2.40 mg/kg, with an average value of 1.68 mg/kg (n = 3). The total Sb concentrations in corn grain were N.D. (not detected) to 35.78 mg/kg, with an arithmetic mean value of 3.18 mg/kg (n = 16) (Ye et al., 2018). The Sb concentration in corn grains in this study was lower than that in the existing XKS study. The concentrations of Sb in crop grain ranged from 0.74 to 8.51 mg/kg, with an average content of 2.23 mg/kg in the largest Hg-Sb mine area in Qinling orogenic belt, China (Qin et al., 2022). Corn grain and sweet potato exhibited different Sb accumulation capacities. The total concentration of Sb in sweet potato was 1.32 and 9.56 mg/kg, with an average value of 5.44 mg/kg (n = 2), which exceeded the limit of 0.04 mg/kg developed by the Joint FAO/WHO Expert Committee on Food Additives (JECFA, 2011). This value is higher than the total Sb concentrations reported by Ye et al. (2018) in sweet potatoes from XKS (0–3.52 mg/kg, mean value 1.2 mg/kg, n = 14). However, China has no toxicity guidelines for Sb concentrations in food.

Buy me a coffee https://ko-fi.com/jurnalin https://dbook.eu.org

Sb chemical speciation in environment matrices

The Sb chemical species in the soil, sediment, river water, tailings, rock, and dust were investigated. Sb(V) was the major Sb species in the soil, with an average of 7.83 mg/kg (Table 2). The chemical valence of Sb in the soils from the XKS mine was dominated by Sb(V) (0.59–10.15%), and the proportion of Sb(III) ranged from 0.001 to 0.04% (Okkenhaug et al., 2011). Sb(III) was relatively low compared to Sb(V) in soil samples from XKS (Wei et al., 2015). Sb(V) identified only in two sediment samples was 1.81 and 9.13 mg/kg, respectively (Table 2). Liang et al. (2018) reported that Sb(III) in sediment from XKS ranged from 0.62 to 549 mg/kg, with an average of 254 mg/kg, and Sb(V) ranged from 9.61 to 5005 mg/kg, with an average of 1311 mg/kg. Sb(III) accounts for < 30% of inorganic Sb [Sb(III) + Sb(V)] in sediments (Liang et al., 2018). Wang et al. (2011) found that Sb(V) was the predominant form in sediments from XKS. Inorganic species Sb(III) and Sb(V) were detected in the tailings and dust, and Sb(V) was present in far greater proportions than Sb(III) (Table 2). In this study, TMSb was below the detection limit in environmental samples from any of the sites. Other studies have detected TMSb only in a few rhizosphere soils (Wei et al., 2015). Three Sb chemical species were all below the detection limits in the rock.

Table 2 Sb chemical speciation in environmental matrices samples (mg/kg, except river water: μg/L). S-soil, Se-sediment, W-river water, T-tailing, R-rock, D-dust

Samples	Sb(III)	Sb(V)	TMSb	TSb
S3	< 0.2	0.89	< 0.2	115
S4	< 0.2	20.8	< 0.2	1115
S7	< 0.2	27.5	< 0.2	837
S10	< 0.2	0.84	< 0.2	195
S13	< 0.2	1.48	< 0.2	65.3
S15	< 0.2	9.11	< 0.2	561
S16-1	< 0.2	6.05	< 0.2	1671
S17-2	< 0.2	0.80	< 0.2	304
S19	< 0.2	3.04	< 0.2	294
Se2	< 0.2	< 0.2	< 0.2	209
Se3	< 0.2	9.13	< 0.2	3032
Se4	< 0.2	1.81	< 0.2	884
W3	< 0.1	0.693	< 0.5	0.68
W5	< 0.1	1.104	< 0.5	1.20
T1	5.99	116.8	< 0.2	1537
R1	< 0.2	< 0.2	< 0.2	1.18
D2	0.258	26.3	< 0.2	1377

Based on the modified BCR sequential extraction, the concentrations of various phases of Sb in soils followed the order: residual fraction (F4) (13.97–84.07%) > oxidizable fraction (F3) (6.96–50.22%) > reducible fraction (F2) (2.87%–67.17%) > exchangeable fraction (F1) (1.87 to 22.46%) (Fig. S4). The modified BCR results showed that the Sb concentrations were mainly associated with the residual fraction, except for samples S3 (F3 proportion reached 50.22%) and S7 (F2 proportion reached 67.17%), which implies that despite the high Sb concentrations in the soil, geochemical mobility was comparatively low. The residual fraction contained the largest amount of Sb, indicating most Sb was incorporated into crystalline minerals (e.g., goethite) or formed Sb-bearing secondary minerals (e.g., tripuhyite). The distinctive Sb species fractions in S3 and S7 were helpful in collaboratively performing pollution source apportionment from a microscopic perspective. This result of the Sb species fraction was not consistent with the literature available on the Sb fraction in soil from XKS. The proportions of Sb fractions in the soil followed the order F4 (96.2–99.6%) > F2 (0.25–2.7%) > F1 (0.09–0.92%) > F3 (0.01–0.15%) (Zhou et al., 2024). A probable cause of the soil with much higher residual Sb was that soils sampling sites existed pollution sources nearby (Zhou et al., 2024).

Mineral composition and in situ distribution of Sb in soil

The mineral composition of the soil samples was analyzed qualitatively and quantitatively. Based on XRD qualitative analysis, the major mineralogical components of the S4 sample from XKS were quartz (SiO_2), dolomite, calcite, kaolinite, muscovite, and montmorillonite (Fig. 3). Dolomite and calcite were the major buffering carbonate minerals. Based on TIMA quantitative analysis, the dominant mineralogical components of the S4 sample from XKS included SiO_2 (59.80%), kaolinite (9.93%), calcite (6.08%), albite (3.41%), chlorite-clinochlore (2.89%), clay (1.99%), dolomite (1.81%), and hematite (Fe_2O_3)/magnetite (Fe_3O_4) (1.67%) (Fig. 4). TIMA analysis results

Buy me a coffee https://ko-fi.com/jurnalin https://dbook.eu.org

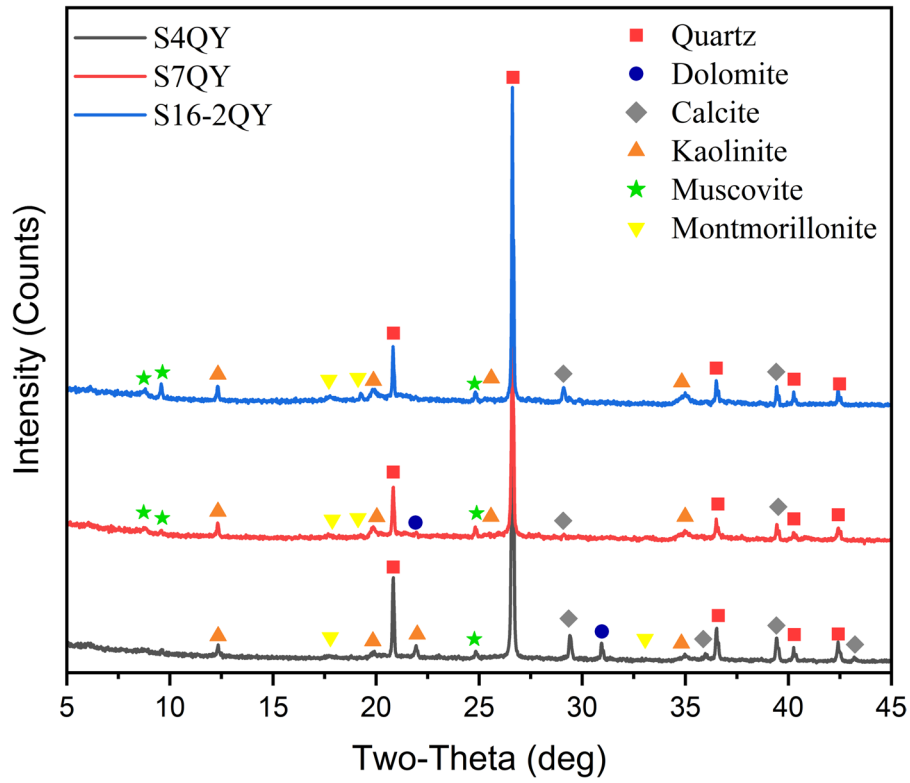

Fig. 3 XRD diffractograms of soil samples from the XKS Sb mine

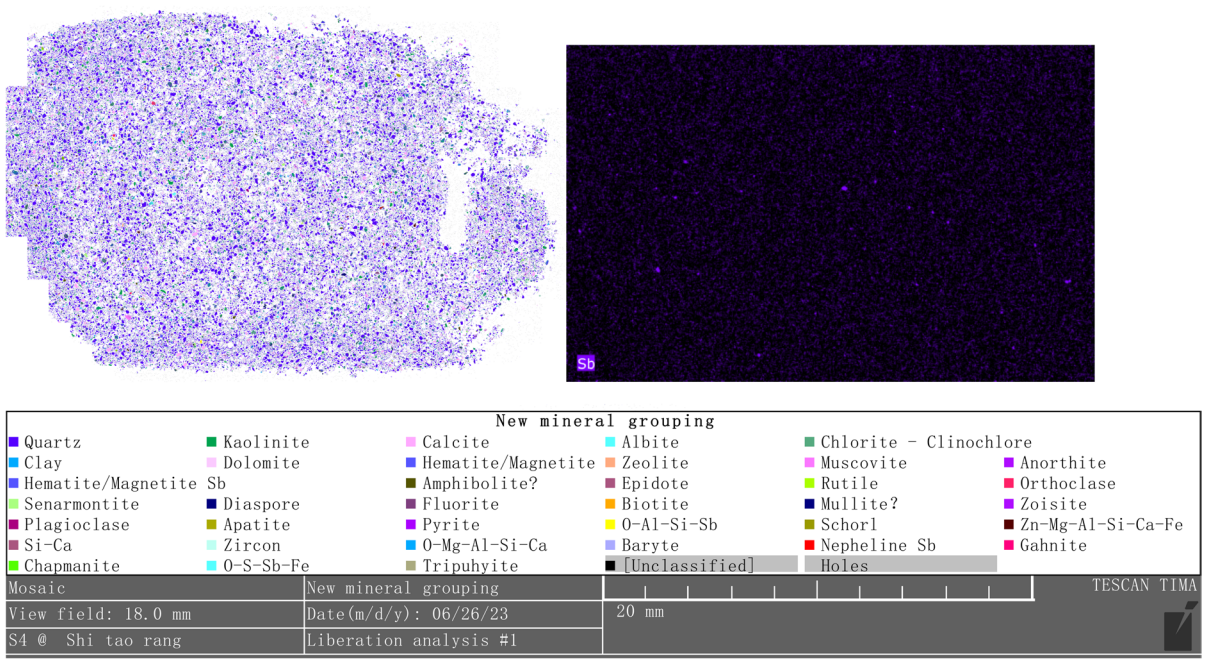

Fig. 4 TIMA characterization of soil sample (S4) from the XKS Sb mine

Buy me a coffee https://ko-fi.com/jurnalin https://dbook.eu.org

were similar to those of XRD analysis. Furthermore, Sb was observed to be associated with Fe_2O_3/Fe_3O_4, nepheline ($NaAlSiO_4$), as well as Sb-bearing minerals consisting of O–Al-Si or O-S-Fe (Fig. 4). It has been proved that Sb in the soil from XKS combined with Fe in the form of tripuhyite ($FeSbO_4$), and complexed with shared edge and corner on the ferrihydrite and goethite (Zhou et al., 2024). Fe (hydr)oxides (such as ferrihydrite, goethite, and hematite) considerably influence Sb migration in soil owing to their strong adsorption of Sb (Yan et al., 2022). Thus, Fe (hydr) oxides and clay minerals in soils are essential for controlling the migration of Sb through surface adsorption and coprecipitation (Drahota et al., 2023).

Based on XRF analysis (Fig. S5), for soil samples S16-1 and S7, the top seven primary elements were O, Si, Al, Fe, K, Ca, Ti, with Sb (accounting for 0.44% and 0.21%) ranking No. 10 and No. 11, respectively. However, for soil sample S4, the top seven primary elements were O, Si, Al, Fe, Ca, K, and Sb (0.78%). In this study, we further used a combination of TIMA and μ-XRF analyses to determine in situ distribution of Sb and associated elements incorporated into different carrier minerals in representative soil sample. Based on the XRF analysis results, the S4 soil sample with a higher Sb proportion than the S7 and S16-1 samples was selected for further μ-XRF analysis. For soil sample S4, based on correlation analysis using μ-XRF analysis results, it can be found that the scanning energy range of Sb LB-edges was associated significantly with that of Al K-edges, Fe KA-edges, S KA-edges, and Si KA-edges ($p < 0.05$) (Fig. 5). The correlation coefficients (R^2) of the scanning energy range for Al-Sb, Fe-Sb, S-Sb, and Si-Sb were 0.2197, 0.2136, 0.1691, and 0.1632, respectively. Aluminum minerals are rich in the soil and strongly control Sb mobility (Essington et al., 2017). The fate of Sb is generally linked to the geochemical cycling of Fe and S (Arsic et al., 2018). Silicified limestone is the major rock-forming mineral in Sb ores. The dissolution of silicate minerals promoted the Sb_2S_3 reaction and increased the Sb(V) content. In addition, calcium antimonate precipitation was found in the XKS soil and controlled Sb concentration in the soil (Okkenhaug et al., 2011). However, in this study, insignificant association between the scanning energy range of Ca and Sb was observed, which implies less important of Sb-Ca co-precipitation compared with the complexation of Sb on Fe oxide surfaces.

Sb isotopic signature in environment matrices

Sb isotope measurements were performed on rock, soil, sediment, river water, dust, tailings, and crop (corn grain and sweet potato) samples from XKS. Crop, dust, rock, soil, sediment, tailings, and river water samples from the XKS Sb mine displayed positive $\delta^{123}Sb$ values; however, the $\delta^{123}Sb$ values

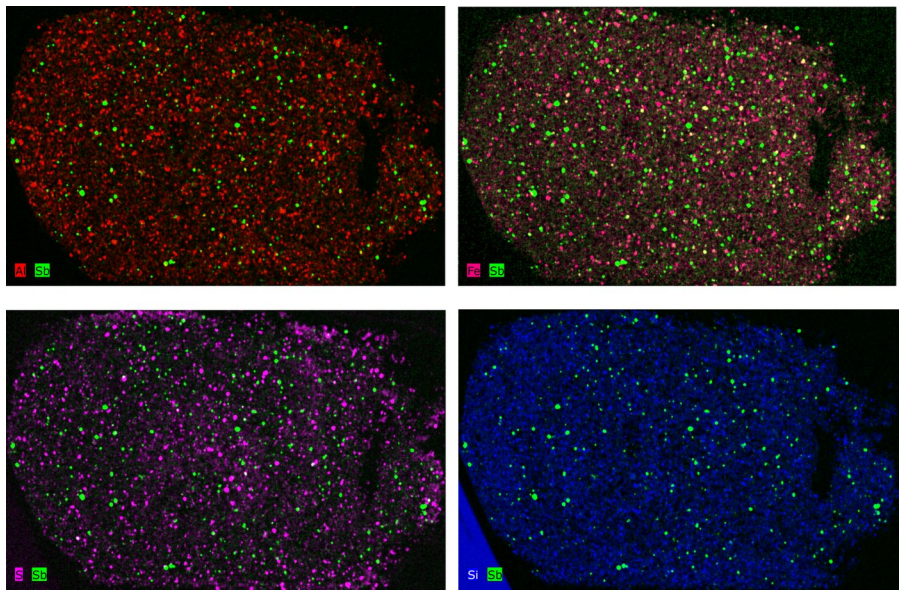

Fig. 5 μ-XRF characterization of soil sample (S4) from the Xikuangshan Sb mine

Buy me a coffee https://ko-fi.com/jurnalin https://dbook.eu.org

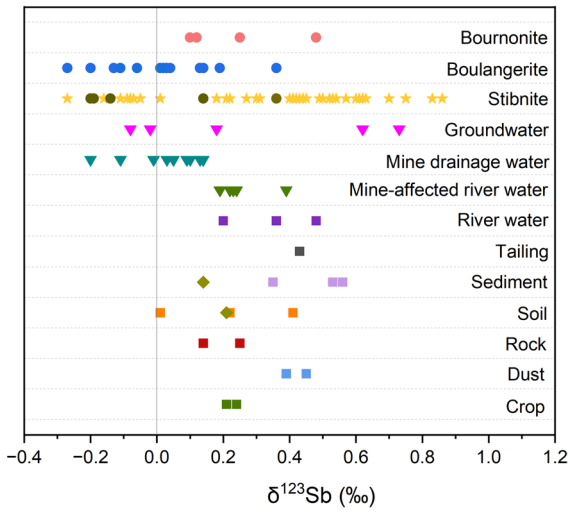

Fig. 6 Antimony isotopic composition in different environmental samples. The data were compiled from Liu et al. (2020) (diamonds), Wang et al., (2021a, 2021b) (circles), Wen et al., (2023a, 2023b) (inverted triangles), and Zhai et al. (2021) (stars), and reported in this study (squares)

in groundwater, mine drainage water, and stibnite samples based on Zhai et al. (2021) and Wen et al., (2023a, 2023b) varied over a wide range (Fig. 6). The Sb isotopic composition of natural sources tends to be negative or close to zero, whereas that of anthropogenic sources tends to be positive (Tanimizu et al., 2011).

River water

The δ^{123}Sb values of river water from the XKS Sb mine were 0.20‰, 0.36‰, and 0.48‰ in this study, which are almost identical to the published Sb isotope data for river water. Wen et al., (2023a, 2023b) reported that the δ^{123}Sb values of mine-affected river waters from the XKS Sb mine ranged from 0.19 to 0.39‰. Resongles et al. (2015) reported that rivers affected by mining activities had a wide range of Sb isotope composition (0.06–0.83‰). Compared with river water, mine drainage water is featured by relatively high Sb concentrations and low δ^{123}Sb values, from −0.2 to 0.14‰ (Wen et al., 2024). Stibnite oxidative dissolution may result in low δ^{123}Sb values (Wen et al., 2024).

In this study, river water from different sites exhibited remarkably different Sb isotopic signatures, which may indicate multiple sources and influence factors for Sb migration in different locations. The Sb isotopic signature of river water sample W3 (0.20‰) matched that of the rock (0.14‰ and 0.25‰), suggesting a similar source or isotope fractionation mechanism of Sb. This indicates that Sb in river water sample W3 may be influenced by rock weathering. Stronger water–rock interactions are the predominant Sb sources for river water (Hao et al., 2022).

Sediment

The δ^{123}Sb values of sediment samples were 0.35‰, 0.53‰, and 0.57‰, corresponding to Sb concentrations of 1,361 mg/kg, 3032 mg/kg, and 209 mg/kg, respectively. Liu et al. (2024a) showed that the δ^{123}Sb values in the sediments from the XKS Sb mine were 0.31–0.56‰. The range of Sb isotopic compositions in this study was comparable to that of the sediment from the XKS Sb mine. The Sb isotopic composition displayed minimal variation, whereas the Sb concentration displayed considerable variation, with variation coefficients of 19.6% and 75.6%, respectively. This indicated that the geochemical behavior of Sb varied under the influence of mining activities (Liu et al., 2024a). Based on relevant studies in XKS, Wen et al., (2023a, 2023b) and Liu et al. (2024a) reported that dilution of Sb along the river and weak adsorption of Sb by sediments do not lead to notable Sb isotopic fractionation in sediment. Notably, the trend of Sb isotope characteristics was opposite to that of Sb concentration for Se2, that is, higher δ^{123}Sb values (0.57‰) corresponded to lower Sb concentrations (209 mg/kg). The Sb concentration in the surface water corresponded to Se2 was low, with an Sb concentration of 1.4 μg/L. Antimony dynamics in sediments are more complex than those in surface water.

The sediment had relatively high δ^{123}Sb values compared to those in other environmental samples and those of stibnite (Fig. 6). In the XKS mine, the δ^{123}Sb values of stibnite showed a wide range (Zhai et al., 2021), which may be referable to separation of stibnite from an Sb-bearing fluid. It was deduced that Sb in the sediment may be related to stibnite. Weathering waste rock particles may enter the sediment, causing changes in the δ^{123}Sb values in the sediment (Resongles et al., 2015). However, the corresponding data of Sb concentration to δ^{123}Sb values in stibnite is not available based on previous studies. Previous studies have documented mine tailings as a common

Buy me a coffee https://ko-fi.com/jurnalin https://dbook.eu.org

source of Sb in sediment (Wang et al., 2011). The δ^{123}Sb values of sediment and tailings (0.44‰) cannot directly deduce the potential influence of tailing weathering on the δ^{123}Sb signature in the sediment in this study. Based on Sb isotopes in sediment sample Se4 (0.53‰) and the corresponding river water sample W3 (0.2‰), sediments tended to enrich heavier Sb isotopes, with enrichment of lighter Sb isotopes in the river water. Given the limited Sb isotope measurement data in this study, further research regarding the fractionation mechanism at the river-sediment interface is required.

Soil

The δ^{123}Sb values of soils from the XKS mine were 0.008‰, 0.221‰, and 0.408‰, which are comparable to those reported for Sb isotope composition in soil. The δ^{123}Sb values in soil profile near abandoned smelters ranged from −0.045 − 0.48‰, 0.009 − 0.36‰, and 0.12 − 0.85‰, respectively from Xihe County, Gansu Province and Qinglong County, Guizhou Province (Li et al., 2025). The δ^{123}Sb value of soil at 0–10 cm was 0.49‰ from Dushan Sb mine, China (Liao et al., 2023). The δ^{123}Sb values of the geological reference materials yellow–red soil were 0.19‰ and 0.23‰ (Liu et al., 2020). A large variation was observed in the δ^{123}Sb values of the soil samples in this study. This suggests that Sb in soils located in different places may have a different origin or migration behavior. The δ^{123}Sb value of soil sample S4 (0.41‰) was close to those of dust (0.39‰ and 0.45‰), tailings (0.44‰), and river water W5 (0.48‰). The elevated Sb concentrations in S4 were inferred to be derived from atmospheric deposition, tailing leaching, and river water surface runoff. The δ^{123}Sb value of soil S3 (0.22‰) was similar to those of river water W3 (0.20‰) and rock R1 (0.25‰). It was assumed that river water surface runoff and rock weathering caused increased Sb concentrations in S3.

The δ^{123}Sb values did not correlate with Sb concentrations in the soil. Soil sample S7, with a high Sb concentration, had a low δ^{123}Sb value (0.01‰). Sample S7 exhibited high Sb(V) (Table 2) and reducible fraction concentrations (Fig. S4). The chemical species of Sb may affect its fractionation in the soil. Previous studies have shown that stibnite oxidized to the oxidation state (Sb_2O_5) result in a lighter Sb isotope composition (decreasing δ^{123}Sb values of 0.25‰) (Dillis et al., 2019). Iron (hydrogen) oxides in the soil preferentially adsorb light Sb isotopes, whereas heavy Sb isotopes are usually present in soil pore water in the form of anions and infiltration with pore water (Wu et al., 2024). Araki et al. (2009) conducted a laboratory experiment on the adsorption of $Sb(OH)_6$ on ferrihydrite, and observed that ^{121}Sb isotope was preferably adsorbed whereas heavier isotopes was slightly enriched in the aqueous phase.

To identify the sources of various environmental matrices samples, the relationship between the δ^{123}Sb value and Sb concentration was established in a two-dimensional coordinate system (Fig. 7). Soil, tailings and road dust showed the same sources. In addition, Sb in soil was derived mainly from the river water surface runoff and rock weathering.

Crop

The Sb isotopic compositions of the edible plant parts of sweet potato and maize harvested around the XKS mine area were 0.24‰ and 0.21‰, respectively. In addition to Mg isotopes, most plants tend to be enriched in light isotopes (Liao et al., 2023). Biological processes can cause isotopic fractionation, such as Cd (Wiggenhauser et al., 2016). However, the fractionation of Sb isotopes in the biological process has not been reported. Sweet potato exhibited a similar Sb isotopic signature (0.24‰) to soil sample S3

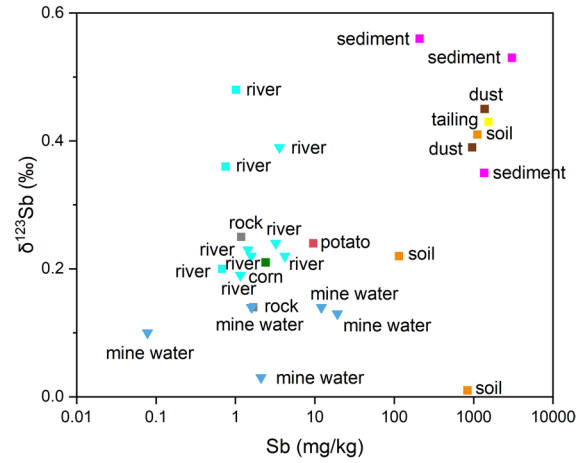

Fig. 7 Variation in δ^{123}Sb values with Sb concentrations in different environmental samples. The data are compiled from Wen et al., (2023a, 2023b) (inverted triangles) and this study (squares)

Buy me a coffee https://ko-fi.com/jurnalin https://dbook.eu.org

(0.22‰), which demonstrated that the sweet potato absorbed Sb through contaminated soil to the root. Studies have shown that atmospheric PTEs enter plants mainly via leaf uptake in polluted smelting areas, and litter may be an indirect input route for the dry deposition of Sb into soil (Liu et al., 2022). Mercury in maize grain from Xunyang Hg-Sb mine was mainly derived from the atmosphere (Shi et al., 2023). In this study, Sb in maize grain (0.21‰) was isotopically lighter than Sb in dust (0.39‰ and 0.45‰). A straight substitution of dust for atmospheric deposition may not be reasonable. Further research is needed to trace Sb in maize grain from atmospheric deposition.

Conceptual model

Conceptual models explaining Sb pollution sources and mobility in different environmental matrices in the XKS Sb mine area were proposed (Fig. 8). Antimony in river water sample W3 may have been influenced by rock weathering. It was concluded that the major source contributing to SO_4^{2-} was the direct oxidative dissolution of stibnite ores in W1 and W2. Weathering waste rock particles may enter the sediment, causing variations in δ^{123}Sb values in the sediment. The Sb concentrations in S4 were derived from atmospheric deposition, tailing leaching, and river water surface runoff, whereas river water surface runoff and rock weathering caused increased Sb concentrations in S3. The oxidation of stibnite and mineral (such as Fe oxides) adsorption may have resulted in the lighter Sb isotope composition in S7. Antimony in street dust is primarily derived from tailing heaps and resuspended soil. Sweet potatoes absorb Sb from contaminated soil to the roots.

Conclusion and perspective

This study adopted a combination of TIMA, μ-XRF, and Sb stable isotopes to elucidate Sb pollution characteristics and the long-distance migration of Sb in environmental matrices from the largest Sb mine in the world. Hematite (Fe_2O_3)/magnetite (Fe_3O_4), nepheline ($NaAlSiO_4$), and Sb-bearing minerals consisting of O-Al-Si or O-S-Fe were rich in Sb in the soil. Antimony in the soil was

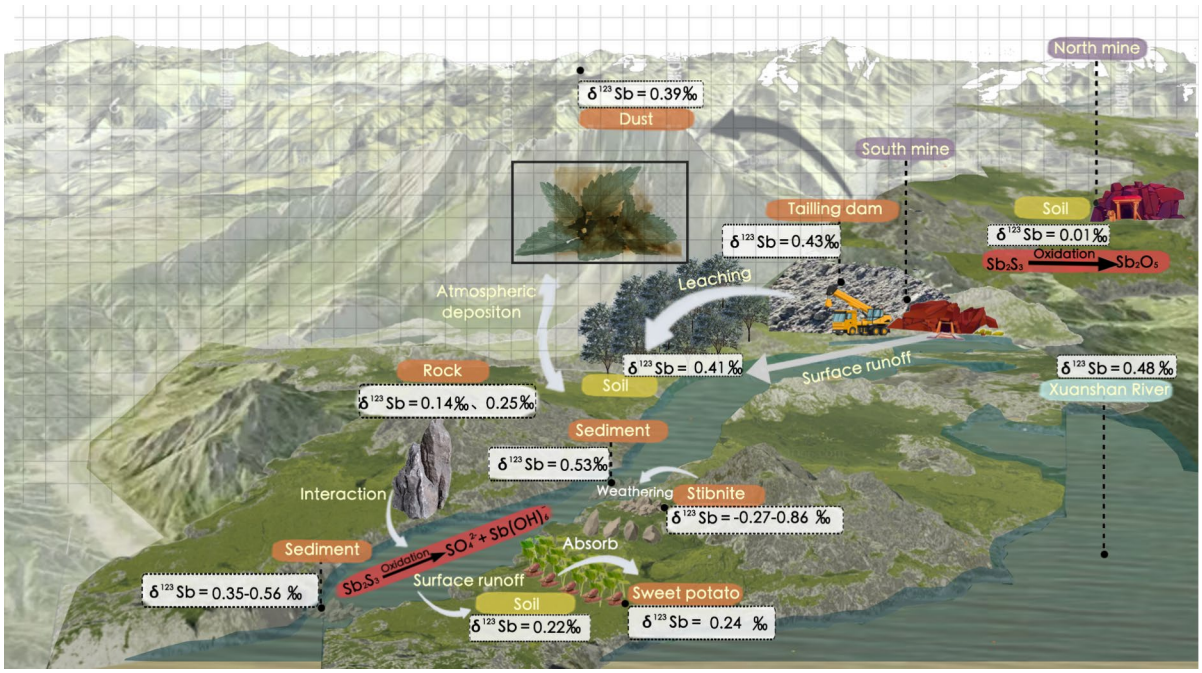

Fig. 8 Conceptual models explaining Sb pollution sources and mobility in different environmental matrices in the XKS Sb mine area

Buy me a coffee https://ko-fi.com/jurnalin https://dbook.eu.org

associated with Al, Fe, S, and Si, which influence Sb mobility. Notable changes were observed in the Sb isotopic composition of soils from the XKS Sb mine area. The Sb isotope composition of the soil was affected by atmospheric deposition, tailing leaching, river water surface runoff, and rock oxidative weathering. The differences in hydrochemical types and Sb isotopic signatures among river waters indicated multiple sources and factors influencing Sb mobilization in different locations. Sweet potatoes absorbed Sb from contaminated soil to the roots. Soil erosion and tailings were the major sources of Sb in street dust. In this study, various geochemical processes affecting Sb transfer were revealed, and the sources and migration models of Sb in the environment in XKS were proposed. This study confirmed the application of Sb isotopes as environmental tracers with suitable evidence, and the Sb isotope method may be suitable for other regions with similar conditions.

However, the Sb isotopes of atmospheric deposition and stibnite were not determined because of the lack of samples collected during the initial experimental design and sampling. The contents of active Fe/Al (hydrogen) oxides and clay minerals in the environmental matrices were not determined. Further studies on the Sb isotope signatures of atmospheric deposition and stibnite, as well as soil parent material from the XKS Sb mine, are needed to quantitatively identify the impact of natural factors coupling anthropogenic activities on Sb pollution in this area.

Acknowledgements We gratefully acknowledge financial support from the support of the Natural Science Foundation of China (No. 42207438, 42207276), and the GDAS' Project of Science and Technology Development (2022GDASZH-2022010104-2).

Author contributions Taoran Shi: formal analysis; Funding acquisition; Investigation; Writing-original draft; Writing-review & editing; Wenjing Guo: funding acquisition; Investigation; Guangyi Sun: data curation; Jining Li: resources; Funding acquisition Jin Ma: resources; Validation; Min Sun: Visualization; Yutong Ji: data curation; Chunfa Wu: visualization; Resources; Validation.

Funding Natural Science Foundation of China, 42207438, 42207276, GDAS' Project of Science and Technology Development, 2022GDASZH-2022010104-2.

Data availability No datasets were generated or analysed during the current study.

Declarations

Conflict of interests The authors declare that they have no Conflict of interests.

References

ANZECC, (2000). Australian and New Zealand Guidelines for Fresh and Marine Water Quality V. 1 (chapter 1–7).

Araki, Y., Tanimizu, M., & Takahashi, Y. (2009). Antimony isotopic fractionation during adsorption on ferrihydrite. *Geochimica Et Cosmochimica Acta, 73*(13), A49–A49.

Arsic, M., Teasdale, P. R., Welsh, D. T., Johnston, S. G., Burton, E. D., Hockmann, K., & Bennett, W. W. (2018). Diffusive gradients in thin films reveals differences in antimony and arsenic mobility in a contaminated wetland sediment during an oxic-anoxic transition. *Environmental Science & Technology, 52*, 1118–1127.

Aston, F. W. (1923). The mass-spectra of chemical elements. *The London, Edinburgh, and Dublin Philosophical Magazine and Journal of Science, 45*, 934–945.

Bolan, N., Kumar, M., Singh, E., Kumar, A., Singh, L., Kumar, S., Keerthanan, S., Hoang, S. A., El-Naggarf, A., Vithanage, M., Sarkar, B., Wijesekara, H., Diyabalanage, S., Sooriyakumar, P., Vinu, A., Wang, H. L., Kirkham, M. B., Shaheen, S. M., Rinklebe, J., & Siddique, K. H. M. (2022). Antimony contamination and its risk management in complex environmental settings: A review. *Environment International, 158*, Article 106908.

Chen, L. J., Li, S. Y., Zhang, M. Y., Liu, X., & Zhu, Z. L. (2024). Antimony isotope fractionation during evaporation from Sb chloride solution. *Chemical Geology, 663*, Article 122288.

Chu, J. W., Mao, J. S., & He, M. C. (2019). Anthropogenic antimony flow analysis and evaluation in China. *Science of the Total Environment, 683*, 659–667.

Cidu, R., Dore, E., Biddau, R., & Nordstrom, D. K. (2018). Fate of antimony and arsenic in contaminated waters at the abandoned Su Suergiu mine (Sardinia, Italy). *Mine Water and the Environment, 37*, 151–165.

CNEMC, China National Environmental Monitoring Center. (1990). *The background concentrations of soil elements of China*. China Environmental Science Press.

Crommentuijn, T., Polder, M., van de Plassche, E.J., (1997). Maximum permissible concentrations and negligible concentrations for metals, taking background concentrations into account. RIVM Rapport 601501001.

Dillis, S., Ham-Meert, A. V., Leeming, P., Shortland, A., Gobejishvili, G., Abramishvili, M., & Degryse, P. (2019). Antimony as a raw material in ancient metal and glass making: Provenancing Georgian LBA metallic Sb by isotope analysis. *STAR: Science & Technology of Archaeological Research, 4*, 1–15.

Drahota, P., Venhauerova, P., & Strnad, L. (2023). Speciation and mobility of arsenic and antimony in soils and mining wastes from an abandoned Sb-Au mining area. *Applied Geochemistry, 152*, Article 105665.

Buy me a coffee https://ko-fi.com/jurnalin https://dbook.eu.org

Essington, M., Stewart, M., & Vergeer, K. (2017). Adsorption of antimonate by kaolinite. *Soil Science Society of America Journal, 81*, 514–525.

Ferrari, C., Resongles, E., Freydier, R., & Casiot, C. (2024). Antimony isotope fractionation during Sb(V) and Sb(III) adsorption on secondary Fe-minerals (schwertmannite, ferrihydrite) typical of mine waters. *Applied Geochemistry, 163*, Article 105935.

Ferrari, C., Resongles, E., Héry, M., Désoeuvre, A., Freydier, R., Delpoux, S., Bruneel, O., & Casiot, C. (2023). Antimony isotopic fractionation during Sb(III) oxidation to Sb(V): Biotic and abiotic processes. *Chemical Geology, 641*, Article 121788.

Fu, S. L., Hu, R. Z., Yin, R. S., Yan, J., Mi, X. F., Song, Z. C., & Sullivan, N. A. (2020). Mercury and in situ sulfur isotopes as constraints on the metal and sulfur sources for the world's largest Sb deposit at Xikuangshan, southern China. *Mineralium Deposita, 55*, 1353–1364.

Fu, Z. Y., Wu, F. C., Mo, C. L., Deng, Q. J., Meng, W., & Giesy, J. P. (2016). Comparison of arsenic and antimony biogeochemical behavior in water, soil and tailings from Xikuangshan, China. *Science of the Total Environment, 539*, 97–104.

Gaiss, S., Amarasiriwardena, D., Alexander, D., & Wu, F. C. (2019). Tissue level distribution of toxic and essential elements during the germination stage of corn seeds (*Zea mays*, L.) using LA-ICP-MS. *Environmental Pollution, 252*, 657–665.

García-Lorenzo, M. L., Martínez-Sánchez, M. J., Pérez-Sirvent, C., LópezSánchez, J., Molina-Ruiz, J., Tudela, M. L. (2015). Geogenic distribution of arsenic (As) and antimony (Sb) in soils of the Murcia region in Spain. *Environmental forensics, 16*, 88–95.

Guo, W. J., Fu, Z. Y., Wang, H., Song, F. H., Wu, F. C., & Giesy, J. P. (2018). Environmental geochemical and spatial/temporal behavior of total and speciation of antimony in typical contaminated aquatic environment from Xikuangshan, China. *Microchemical Journal, 137*, 181–189.

Hao, C. M., Liu, M., Peng, Y. G., & Wei, Z. B. (2022). Comparison of antimony sources and hydrogeochemical processes in shallow and deep groundwater near the Xikuangshan mine, Hunan Province, China. *Mine Water and the Environment, 41*, 194–209.

He, M. C., Wang, X. Q., Wu, F. C., & Fu, Z. Y. (2012). Antimony pollution in China. *Science of the Total Environment, 421–422*, 41–50.

Herath, I., Vithanage, M., & Bundschuh, J. J. (2017). Antimony as a global dilemma: Geochemistry, mobility, fate and transport. *Environmental Pollution, 223*, 545–559.

JECFA, (2011). Joint FAO/WHO Expert Committee on Food Additives Seventy-fourth meeting Rome, 14–23 June 2011. Retrieved from: http://www.fao.org/3/a-at873e.pdf (23.08.2018).

Jia, X. C., Kaufmann, A., Lazarov, M., Wen, B., Weyer, S., Zhou, J. W., Ma, L. Y., & Majzlan, J. (2024). Antimony isotope fractionation during kinetic Sb(III) oxidation by antimony-oxidizing bacteria *Pseudomonas sp.* J1. *Environmental Science & Technology, 58*, 11411–11420.

Kaufmann, A. B., Lazarov, M., Horn, I., Števko, M., Đorđević, T., Kiefer, S., Weyer, S., & Majzlan, J. (2024). Weathering-induced Sb isotope fractionation during leaching of stibnite and formation of secondary Sb minerals. *Chemical Geology, 662*, Article 122253.

Li, L., Liu, H., & Li, H. X. (2018). Distribution and migration of antimony and other trace elements in a karstic river system, Southwest China. *Environmental Science and Pollution Research, 25*, 28061–28074.

Li, X. Y., Sun, G. Y., Lin, Y., Wu, Y. J., Cheng, Y., Fu, C. L., Chen, Y., & Feng, X. B. (2025). Application of antimony stable isotopes in revealing the source and vertical migration of Sb in soil. *Environmental Science & Technology, 59*, 6285–6296.

Li, Y. B., Guo, L. F., Häggblom, M. M., Yang, R., Li, M. Y., Sun, X. X., Chen, Z., Li, F. B., Su, X. F., Yan, G., Xiao, E. Z., Zhang, H. H., & Sun, W. M. (2022). *Serratia* spp. are responsible for nitrogen fixation fueled by As(III) oxidation, a novel biogeochemical process identified in mine tailings. *Environmental Science & Technology, 56*, 2033–2043.

Li, Z. Y., Ma, Z. W., van der Kuijp, T. J., et al. (2014). Comprehensive comparison of probabilistic health risks of soil heavy metals in China's mining areas. *Science of the Total Environment, 468*, 843–853.

Liang, Z. W., Hua, Z. S., Jia, P., Liu, J., Luo, Z. H., Chen, W. C., Kuang, J. L., Liao, B., Shu, W. S., & Li, J. T. (2018). Strong associations between biogeochemical factors and Sb species in sediments of the world's largest Sb mine (Xikuangshan) in China. *Journal of Geophysical Research: Biogeosciences, 123*, 1548–1556.

Liao, J., Tan, D., Qin, H. B., Han, Q., Liu, E. G., Chen, J. A., Ning, Z. P., & Li, S. H. (2023). Antimony isotope fractionation and the key controls in the soil profiles of an antimony smelting area. *Journal of Hazardous Materials, 454*, Article 131553.

Liu, H.J., Zeng, W., He, M.C., Lin, C.Y., Ouyang, W., Liu., X.T., (2023). Occurrence, distribution, and migration of antimony in the Zijiang River around a superlarge antimony deposit zone. Environ. Pollut. 316, 120520.

Liu, H. J., Sun, G. Y., He, M. C., Feng, X. B., Lin, C. Y., Ouyang, W., & Liu, X. T. (2024a). The composition and differences of antimony isotopic in sediments affected by the world's largest antimony deposit zone. *Water Research, 254*, Article 121427.

Liu, H., Zhou, J., Li, M., Xia, R., Wang, X., & Zhou, J. (2022). Dynamic behaviors of newly deposited atmospheric heavy metals in the soilpak choi system. *Environmental Science & Technology, 56*(17), 12734–12744.

Liu, J. F., Chen, J. B., Zhang, T., Wang, Y. N., Yuan, W., Lang, Y. C., Tu, C. L., Liu, L. Z., & Birck, J. L. (2020). Chromatographic purification of antimony for accurate isotope analysis by MC-ICP-MS. *Journal of Analytical Atomic Spectrometry, 35*, 1360–1367.

Liu, L. H., Tulcan, R. X. S., He, M. C., Ouyang, W., Zhang, Q. W., Yarleque, C. M. H., & Chicaiza-Ortiz, C. (2024b). Antimony pollution threatens soils and riverine habitats across China: An analysis of antimony concentrations, changes, and risks. *Critical Reviews in Environmental Science and Technology, 54*, 797–816.

Nelson, B., Yu-Wei, C., & Montserrat, F. (2011). Human exposure to antimony: I. Sources and intake. *Critical*

Buy me a coffee https://ko-fi.com/jurnalin https://dbook.eu.org

Reviews in Environmental Science and Technology, 41, 1309–1373.

Nyirenda, T. M., Zhou, J. W., Xie, L. N., Pan, X. Z., & Li, Y. (2015). Determination of carbonate minerals responsible for alkaline mine drainage at Xikuangshan Antimony Mine, China: Using thermodynamic chemical equilibrium model. *Journal of Earth Science, 26*, 755–762.

Okkenhaug, G., Zhu, Y. G., Luo, L., Lei, M., Li, X., & Mulder, J. (2011). Distribution, speciation and availability of antimony (Sb) in soils and terrestrial plants from an active Sb mining area. *Environmental Pollution, 159*, 2427–2434.

Pervaiz, A., Zhong, Q. Y., Rehman, S. A. U., Ma, C. L., Jiao, Y. H., & He, M. C. (2023). Immobilization and phytoavailability of antimony (Sb) in contaminated agricultural soils amended with composted manure. *Science of the Total Environment, 856*, Article 159213.

Pierart, A., Shahid, M., Sejalon-Delmas, N., & Dumat, C. (2015). Antimony bioavailability: Knowledge and research perspectives for sustainable agricultures. *Journal of Hazardous Materials, 289*, 219–234.

Qin, Z. M., Zhao, S. T., Shi, T. R., Zhang, F. Y., Pei, Z. R., Wang, Y. H., & Liang, Y. R. (2022). Accumulation, regional distribution, and environmental effects of Sb in the largest Hg–Sb mine area in Qinling Orogen, China. *Science of the Total Environment, 804*, Article 150218.

Radková, A. B., Jamieson, H. E., & Campbell, K. M. (2020). Antimony mobility during the early stages of stibnite weathering in tailings at the Beaver Brook Sb deposit, Newfoundland. *Applied Geochemistry, 115*, Article 104528.

Rauret, G., Lopez-Sanchez, J., Sahuquillo, A., Rubio, R., Davidson, C., Ure, A., & Quevauviller, P. (1999). Improvement of the BCR three step sequential extraction procedure prior to the certification of new sediment and soil reference materials. *Journal of Environmental Monitoring, 1*, 57–61.

Ren, M. Y., Ding, S. M., Fu, Z., Yang, L. Y., Tang, W. Y., Tsang, C. W., Wang, D., & Wang, Y. (2019). Seasonal antimony pollution caused by high mobility of antimony in sediments: In situ evidence and mechanical interpretation. *Journal of Hazardous Materials, 367*, 427–436.

Resongles, E., Freydier, R., Casiot, C., Viers, J., Chmeleff, J., & Elbaz-Poulichet, F. (2015). Antimony isotopic composition in river waters affected by ancient mining activity. *Talanta, 144*, 851–861.

Rouxel, O., Ludden, J., & Fouquet, Y. (2003). Antimony isotope variations in natural systems and implications for their use as geochemical tracers. *Chemical Geology, 200*, 25–40.

Sheng, L. L., Hao, C. M., Guan, S. D., & Huang, Z. B. (2022). Spatial distribution, geochemical behaviors and risk assessment of antimony in rivers around the antimony mine of Xikuangshan, Hunan Province, China. *Water Science and Technology, 85*, 1141–1154.

Shi, T. R., Zhan, P., Shen, Y. Q., Wang, H. Y., Wu, C. F., Li, J. N. (2023). Using multi-technology to characterize transboundary Hg pollution in the largest presently active Hg deposit in China. *Environmental Science and Pollution Research, 30*, 82124–82141.

Song, X. F., Lai, J. Q., Xu, J. W., Liu, X. H., Li, B., He, H. S., Wang, Y. H., Shi, J., Wang, C. F., & Wen, C. H. (2022). Material source and genesis of the Daocaowan Sb deposit in the Xikuangshan ore field: LA-ICP-MS trace elements and sulfur isotope evidence from stibnite. *Minerals, 12*, Article 1407.

Sun, G. Y., Wu, Y. J., Feng, X. B., Wu, X., Li, X. Y., Deng, Q. W., Wang, F. Y., & Fu, X. W. (2021). Precise analysis of antimony isotopic composition in geochemical materials by MC-ICP-MS. *Chemical Geology, 582*, Article 120459.

USGS, (2023). Mineral commodity summaries. Cement Americas.

Wang, D., Mathur, R., Zheng, Y. Y., Qiu, K. F., & Wu, H. J. (2021a). Redox-controlled antimony isotope fractionation in the epithermal system: New insights from a multiple metal stable isotopic combination study of the Zhaxikang Sb–Pb–Zn–Ag deposit in Southern Tibet. *Chemical Geology, 584*, Article 120541.

Wang, H. Z., Cai, L. M., Wang, Q. S., Hu, G. C., & Chen, L. G. (2021b). A comprehensive exploration of risk assessment and source quantification of potentially toxic elements in road dust: A case study from a large Cu smelter in central China. *CATENA, 196*, Article 104930.

Wang, W. Q., Wang, H. M., Cheng, X. Y., Wu, M. X. J., Song, Y. Y., Liu, X. Y., Loni, P. C., & Tuovinen, O. H. (2022). Different responses of bacteria and fungi to environmental variables and corresponding community assembly in Sb-contaminated soil. *Environmental Pollution, 298*, Article 118812.

Wang, X., He, M., Xi, J., & Lu, X. (2011). Antimony distribution and mobility in rivers around the world's largest antimony mine of Xikuangshan Hunan Province, China. *Microchemical Journal, 97*, 4–11.

Wei, C. Y., Ge, Z. F., Chu, W. S., & Feng, R. W. (2015). Speciation of antimony and arsenic in the soils and plants in an old antimony mine. *Environmental and Experimental Botany, 109*, 31–39.

Wen, B., Zhou, A. G., Zhou, J. W., Huang, J. B., Long, T., Jia, X. C., Zhou, W. Q., & Li, W. Y. (2023a). Sources of antimony contamination and its migration into water systems of Xikuangshan, China: Evidence from hydrogeochemical and stable isotope (H, O, S, and Sr) signatures. *Environmental Pollution, 337*, Article 122381.

Wen, B., Zhou, J. W., Tang, P. D., Jia, X. C., Zhou, W. Q., & Huang, J. B. (2023b). Antimony (Sb) isotopic signature in water systems from the world's largest Sb mine, central China: Novel insights to trace Sb source and mobilization. *Journal of Hazardous Materials, 446*, Article 130622.

Wen, B., Zhou, J. W., Zhou, A. G., Liu, C. F., & Li, L. G. (2018). A review of antimony (Sb) isotopes analytical methods and application in environmental systems. *International Biodeterioration & Biodegradation, 128*, 109–116.

Wiggenhauser, M., Bigalke, M., Imseng, M., Müller, M., Keller, A., Murphy, K., Kreissig, K., Rehkamper, M., Wilcke, W., & Frossard, E. (2016). Cadmium isotope fractionation in soil-wheat systems. *Environmental Science & Technology, 50*(17), 9223–9231.

Wu, T. L., Cui, X. D., Cui, P. X., Ata-Ul-Karim, S. T., Sun, Q., Liu, C., Fan, T. T., Gong, H., Zhou, D. M., & Wang, Y. J. (2019). Speciation and location of arsenic and antimony in rice samples around antimony mining area. *Environmental Pollution, 252*, 1439–1447.

Buy me a coffee https://ko-fi.com/jurnalin https://dbook.eu.org

Wu, Y., Sun, G. Y., Huang, J. H., Fan, H. F., Li, X. Y., Zhou, M. Y., Xia, Y., & Feng, X. B. (2024). Antimony isotopic fractionation during intensive chemical weathering of basalt in the tropics. *Geochimica Et Cosmochimica Acta, 367*, 29–40.

Yan, L., Chan, T., & Jing, C. (2022). Mechanistic study for antimony adsorption and precipitation on hematite facets. *Environmental Science & Technology, 56*, 3138–3146.

Yang, D. S., Shimizu, M., Shimazaki, H., Li, X. H., & Xie, Q. L. (2006). Sulfur isotope geochemistry of the supergiant Xikuangshan Sb deposit, Central Hunan, China: Constraints on sources of ore constituents. *Resource Geology, 56*, 385–396.

Ye, L., Qiu, S. X., Li, X. H., Jiang, Y. X., & Jing, C. Y. (2018). Antimony exposure and speciation in human biomarkers near an active mining area in Hunan China. *Science of the Total Environment, 640–641*, 1–8.

Yu, H. C., Qiu, K. F., Simon, A. C., Wang, D., Mathur, R., Wan, R. Q., Jiang, X. Y., & Deng, J. (2023). Telescoped boiling and cooling mechanisms triggered hydrothermal stibnite precipitation: Insights from the world's largest antimony deposit in Xikuangshan China. *American Mineralogist, 108*, 1213–1223.

Zhai, D. G., Mathur, R., Liu, S. A., Liu, J. J., Godfrey, L., Wang, K. X., Xu, J. W., & Vervoort, J. (2021). Antimony isotope fractionation in hydrothermal systems. *Geochimica Et Cosmochimica Acta, 306*, 84–97.

Zhang, C., Liu, L. B., Chen, X. Y., Dai, Y. C., & Jia, H. Z. (2022a). Mechanistic understanding of antimony(V) complexation on montmorillonite surfaces: Insights from first-principles molecular dynamics. *Chemical Engineering Journal, 428*, Article 131157.

Zhang, D., Guo, J. L., Xie, X. J., Zhang, Y. H., & Jing, C. Y. (2022b). Acidity-dependent mobilization of antimony and arsenic in sediments near a mining area. *Journal of Hazardous Materials, 426*, Article 127790.

Zhou, W. Q., Liu, P., Ye, Z. H., Wen, B., Beckie, R. D., Zhou, A. G., Zhou, Z. Y., & Zhou, J. W. (2024). Antimony mobility in soil near historical waste rock at the world's largest Sb mine, Central China. *Science of the Total Environment, 921*, Article 171194.

Zhou, W. Q., Zhou, J. W., Feng, X. B., Wen, B., Zhou, A. G., Liu, P., Sun, G. Y., Zhou, Z. Y., & Liu, X. (2023). Antimony isotope fractionation revealed from EXAFS during adsorption on Fe (oxyhydr)oxides. *Environmental Science & Technology, 57*, 9353–9361.

Publisher's Note Springer Nature remains neutral with regard to jurisdictional claims in published maps and institutional affiliations.

Springer Nature or its licensor (e.g. a society or other partner) holds exclusive rights to this article under a publishing agreement with the author(s) or other rightsholder(s); author self-archiving of the accepted manuscript version of this article is solely governed by the terms of such publishing agreement and applicable law.

Buy me a coffee https://ko-fi.com/jurnalin https://dbook.eu.org